基于 SYSWELD的 GTAW三维动态熔池形状的有限元模拟

李瑞英[1]，　赵　明[2]，　周鸿雁[1]

（1. 大庆师范学院 物理与电气信息工程学院，黑龙江 大庆　163712；
2. 中国石油大学 机电工程学院，山东 东营　257061）

李瑞英

摘　要：基于双椭球体热源模型，建立了运动电弧作用下的 GTAW焊接不锈钢 0Cr18Ni9薄板三维瞬态焊接热过程的数值分析模型. 考虑了材料的热物理性能参数、相变潜热与温度的非线性关系，给出了应用 SYSWELD软件的校正工具对热源分布参数进行确定的方法. 将熔池形状的有限元解同试验结果进行了比较，计算所得熔池形状与实测结果吻合较好，证明了双椭球体热源模型能够较好地反映 GTAW电弧的热流密度分布.

关键词：双椭球体热源模式；熔池形状；有限单元法；数值模拟

中图分类号：TG444^{+}.74　　文献标识码：A　　文章编号：0253－360X(2011)04－0041－04

0　序　　言

钨极氩弧焊（gas tungsten arc welding，GTAW）是自动化焊接和机器人焊接中最常用的熔焊工艺之一. 焊接过程中的熔池形状及其周围温度场的分布影响着焊缝的几何尺寸及接头的组织和性能，反映了复杂的焊接热过程. 一些研究者只是针对固定电弧的二维瞬态或是三维准稳态问题建立了相应的模型[1－3]，且大多数都是采用平面热源模式，越来越多的研究者开始关注对于焊接熔池的三维瞬态行为，并取得了较好的成果[4].

采用的双椭球体热源模型虽可较好地反映 GTAW焊接电弧的功率密度分布，却因为没有明确的公式来确定双椭球体热源分布参数值该如何选取，需经过大量的试算过程才可能得到较为合理的热源分布参数值. 文中对此原因进行分析，给出了应用 SYSWELD软件的校正工具确定双椭球体热源分布参数的方法. 利用校正所得的双椭球体移动热源模型，对运动电弧作用下 GTAW焊接 3 mm厚不锈钢薄板的焊接过程进行了有限元模拟，预测了平板堆焊时三维瞬态熔池形状的动态演变，并进行了试验验证.

收稿日期：2009－06－08

基金项目：青岛市科技发展计划项目（09－1－3－37－jch）；大庆师范学院自然科学基金资助项目（09ZQ07，08ZQ08）；中国石油大学博士科研基金资助项目（Y070305）

1　数学模型

1.1　温度场控制方程及边界条件

设焊接材料为各向同性，温度 $T(x, y, z, t)$是位置坐标（x, y, z）与时间 t的函数，在间接考虑熔池中液态金属流动的情况下，区域中的任意点应满足能量守恒方程

$$\rho c_p \frac{\partial T}{\partial t} = \frac{\partial}{\partial x}\left(k\frac{\partial T}{\partial x}\right) + \frac{\partial}{\partial y}\left(k\frac{\partial T}{\partial y}\right) + \frac{\partial}{\partial z}\left(k\frac{\partial T}{\partial z}\right) + Q \tag{1}$$

式中：k为热导率；c_p为比定压热容；ρ为材料密度；T为温度；t为时间；Q为源项.

为便于计算，利用 Galerkin法将式（1）写为有限元的形式，即

$$[C]\frac{\partial T}{\partial t}\{T_e\} + [K]\{T_e\} = \{F_e\} \tag{2}$$

式中：$[C]$为热容矩阵；$[K]$为热传导矩阵；$\{F_e\}$为热流矢量；$\{T_e\}$为单元节点温度矢量.

能量守恒方程的边界条件在工件上表面为

$$\left.\begin{aligned} k\frac{\partial T}{\partial z} &= q_a - q_{cr} - q_{evp} \\ q_{cr} &= \alpha_{cr}(T - T_a) \\ q_{evp} &= m_{er} I_b \end{aligned}\right\} \tag{3}$$

式中：q_a为电弧热流密度；q_{cr}是因对流和辐射而散

失的热流密度；q_{vp}是因蒸发而散失的热流密度；α_{cr}为对流和辐射的综合热传导系数；T_a是环境温度；m_{er}为蒸发率；L_b为蒸发潜热常数，对于不锈钢，液气相变潜热为 $L_b=6.259\,5\times10^6$ J/kg[5]．

在工件下表面为

$$-k\frac{\partial T}{\partial z}=-q_{cr} \tag{4}$$

计算区域关于焊缝中心线对称，对于对称面（$y=0$），有

$$\frac{\partial T}{\partial y}=0 \tag{5}$$

能量守恒方程的初始条件为

$$T(x,y,z,0)=T_a \tag{6}$$

1.2 双椭球体热源模型

Goldak[6]提出的双椭球体（double ellipsoid，DE）热源分布模式是一种体热源，认为焊接电弧加热斑点的热源功率密度的分布是以双椭球体移动热源模型来描述的．作用于工件上的体热源沿轴分成前、后两部分是为了能更好的模拟出焊接过程中移动热源的前端和后端不同的温度梯度分布（前端较陡，后端较缓），模型考虑了焊接电流的挖掘与搅拌作用，能够反映出束流沿深度方向对焊件进行加热的特点，虽然热流密度函数复杂，参数较多，却有助于得到更为准确的计算结果．具体数学表达式分为沿 y 轴前半部分的椭球体内部热流密度分布

$$q_f(x,y,z)=\frac{6\sqrt{3}(f_f\eta UI)}{ab_1c\pi\sqrt{\pi}}\exp\left(-\frac{3x^2}{a^2}-\frac{3y^2}{b_1^2}-\frac{3z^2}{c^2}\right)$$

$$y\geqslant0 \tag{7}$$

和沿 y 轴后半部分的椭球体内部热流密度分布

$$q_r(x,y,z)=\frac{6\sqrt{3}(f_r\eta UI)}{ab_2c\pi\sqrt{\pi}}\times\exp\left(-\frac{3x^2}{a^2}-\frac{3y^2}{b_2^2}-\frac{3z^2}{c^2}\right)$$

$$y<0 \tag{8}$$

式中：η为电弧热效率；I为焊接电流；U为电弧电压；f_f，f_r分别为总的输入功率在熔池前、后两部分的分配系数；a，b_1，b_2，c分别为双椭球体热源形状参数，参见文献[7]．

1.3 热源分布参数的确定

双椭球体热源模型的参数值是根据经验以及试验结果来确定的．运用 SYSWELD软件的校正工具对热源分布参数进行确定步骤如下．

（1）首先根据经验对形状参数取初值进行试算．初值的选定可根据达到准稳态情况下的试验测试值的比例来选定．例如测得某一具体的焊接工艺条件下达到宏观准稳态时，熔池长度∶熔宽∶熔深＝10∶8∶2，则双椭球体热源形状参数之间的关系满足 $2a:(b_1+b_2):2c=8:10:2$，于是可预设 $a:b_1:b_2:c=4:4:6:1$或 $4:4.5:5.5:1$或 $4:3:7:1$等．

（2）将试算所得温度场结果与试验结果进行对比，针对具体的焊接工艺，判断应调整 a，b_1，b_2，c中的某个形状参数值：①是将该参数值增大还是减少；②还是该将所有形状参数值 a，b_1，b_2，c同比增大或同比缩小，最终确定合适的形状参数值．

（3）对于热源模型另外一个很重要的参数——输入能量 Q_0的确定也是有一定规律可循的．试算时，任意输入一个能量值 Q_1，对应得到一个输出能量 Q_2（最终加载到工件上的能量）．按实际要求输出能量为 $Q=\eta UI$，则对应的输入能量 Q_0与 Q满足如下关系

$$\frac{Q_1}{Q_0}=\frac{Q_2}{Q} \tag{9}$$

根据式（9）只需试算一次，便可确定热源的输入能量 Q_0的值．

通过上述方法来确定双椭球热源分布参数，可以大大减少试算次数，避免因盲目取值和反复多次试算拼凑而带来的不必要的工作量和低效率，提高数值模拟的计算效率和精度．

2 有限元法

利用 SYSWELD，综合考虑在电弧热流作用下熔池表面蒸发散热、熔池内部对流散热、熔池固液界面的相变潜热等各种因素，求解上述控制方程及定解条件．被焊工件为奥氏体不锈钢 0Cr18Ni9，尺寸为 200 mm×60 mm×3 mm，热物理性能参数的取值见表 1．在数值模拟中，假定工件表面与空气的换热系数为 25 W/(m²·K)．

表 1 材料 0Cr18Ni9的热物理性能参数

Table 1 Thermal physical parameters of 0Cr18Ni9

物理量名称	物理量/单位	取 值
环境温度	T_∞/K	293
液相线温度	T_l/K	1 723
固相线温度	T_s/K	1 523
线膨胀系数	β/K^{-1}	10^{-4}
密度	ρ/(kg·m^{-3})	7 930
重力加速度	g/(m·s^{-2})	9.8
换热系数	h_c/(W·m^{-2}·K^{-1})	80.0
固液相变潜热	ΔH/(J·kg^{-1})	2.6×10^5
表面辐射系数	ε	0.9
液气相变潜热	L_b/(J·kg^{-1})	$6.259\,5\times10^6$

数值模拟的精度不仅取决于模型，而且与网格的划分有很大关系．在 SYSWELD中，时间步长是

根据网格密度以及焊接工件尺寸自动设置的. 网格的划分既不能太疏也不能太密,太疏则达不到精度要求,太密则会增加计算时间,增加计算机载荷,甚至超出载荷,影响计算结果. 由于熔池关于焊缝中心线对称,为了减少计算量可计算工件的一半. 为保证焊缝及其附近高温区域得到较为精确的温度分布,焊缝附近划分密网格,其它区域为疏网格,如图 1a所示. 为了更好地描述三维焊接温度场的分布,采用 8节点 6面体单元对工件进行网格划分,共划分为 2.59万个单元, 2.3001万个节点,如图 1b所示.

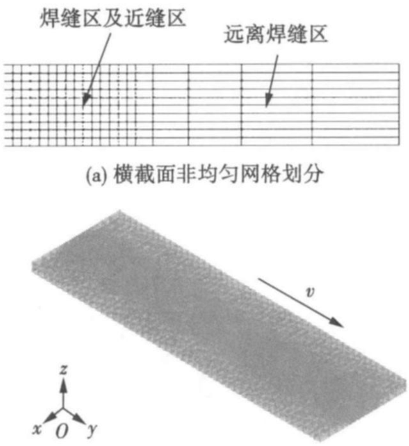

(a) 横截面非均匀网格划分

(b) 工件的有限元网格示意图

图 1　有限元网格示意图

Fig. 1　Schematic of finite element meshes

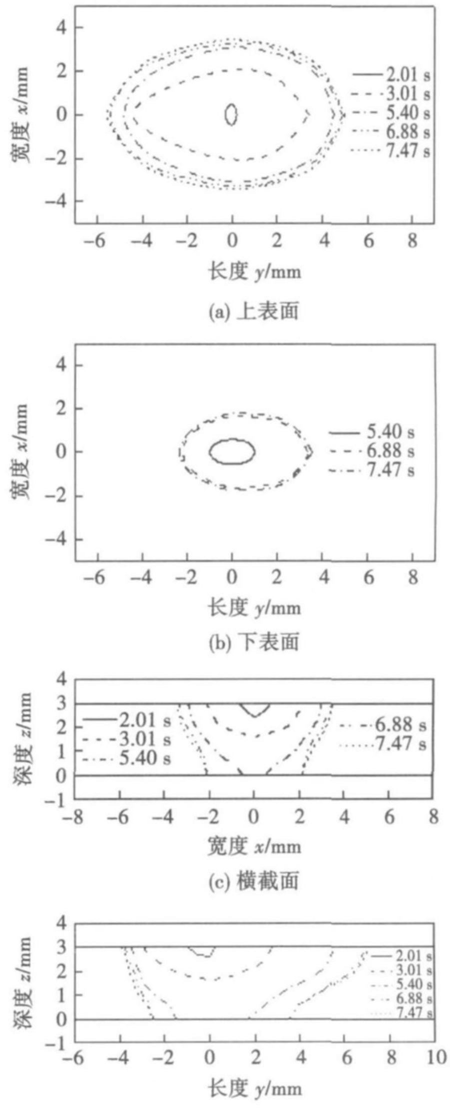

(a) 上表面

(b) 下表面

(c) 横截面

(d) 纵截面

图 2　熔池形状的动态演变

Fig. 2　Transient variation of weld pool geometry

3　计算结果与分析

利用校正好的双椭球体热源模型,针对具体的 GTAW焊接工艺(3 mm厚 0Cr18Ni9; $I=110$ A, $U=12$ V, $v=2$ mm/s)条件,取焊接热效率 $\eta=0.7$,进行有限元数值模拟计算. 从工件上焊接温度场[7]的动态演变图中,通过观察 1 723 K(1 723 K为不锈钢材料 0Cr18Ni9的熔点)等温线随时间的变化情况,可以观察到整个熔池形状的动态变化. 根据焊接温度场的计算结果提取出了熔合线的坐标,为了突出显示熔池形状瞬态变化,便于对比观察,将不同时刻的熔池形状集中到一个图中. 图 2给出了从 2.01 s(熔池开始形成)到 7.47 s(达到宏观准稳态)这一过程不同时刻熔池形状的动态演变过程,分别从工件的上表面、下表面、横截面、纵截面来表征其变化规律.

图 2a为工件上表面熔池形状尺寸随时间的瞬态变化. 可以看出,在焊接开始阶段熔池接近于一个很小的圆. 随着焊接时间的推移和焊枪在工件上的移动,熔池的长度和宽度均逐渐变大,而且长度的变化相对宽度更为明显,因此熔池逐渐变长,并随焊接时间的延长向前移动,熔池的形状逐渐发展成为椭圆形. 原因是在焊接开始阶段,热源相当于一个点热源,熔池形状比较圆;随着时间延长,热源向前移动,使工件在长度方向的热传导加快,熔池变长. 图 2b描述了工件下表面熔池形状的动态演变过程. 可见,在 5.40 s时下表面熔化,工件熔透,这从图 2c与图 2d中均可以看出. 图 2c,图 2d分别为焊缝横截面、纵截面熔池形状尺寸随时间的变化,可以看出,随着时间的延长,熔池逐渐长大,熔宽、熔深和熔池长度均逐渐增加, 7.47 s时熔池形状达到宏观准稳态.

如果将熔池看作一个整体，则熔池的热行为可以简略地认为由两部分能量的变化引起的，即焊接热输入和熔池散热．熔池的散热取决于熔池的大小和温度以及熔池周围的温度．熔池越大、温度越高，则熔池的散热越快；熔池周围温度越高，散热越慢．焊接热输入为固定值，在焊接开始时，熔池较小，熔池内的温度较低，所以熔池散失的热量较少，吸收热量大于散失热量，熔池逐渐长大，散失的热量也逐渐增多，熔池内增加的热量逐渐减少，熔池长大也越来越慢，直到熔池形状几何尺寸达到准稳态，散失的热量与吸收的热量平衡，熔池形状达到准稳态．

图 3 是 GTAW 焊接不锈钢试件所得的接头达到宏观准稳态时焊缝横截面的计算值与实测值的比较，由图可见在不考虑熔池自由表面变形的情况下，上、下表面熔宽以及熔合线在工件内部的形状和走向，计算结果与试验结果基本吻合．

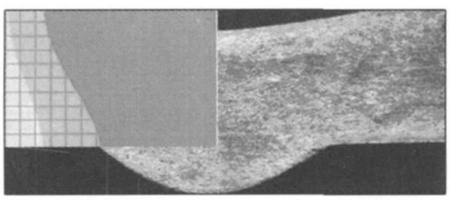

(a) 熔合线形状与走向计算值与实测值的比较

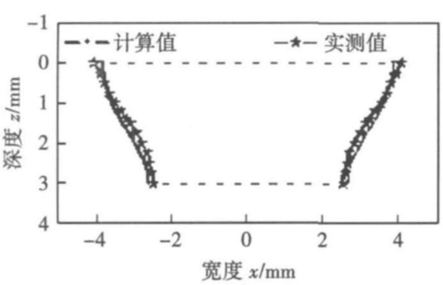

(b) 熔池宽度计算值与实测值的比较

图 3 焊缝横截面计算值与实测值的比较

Fig. 3 Comparison between calculated cross-section of weld pool and experimental one

4 结论

（1）基于 SYSWELD 软件平台，建立了运动电弧作用下 GTAW 焊接 3 mm 厚不锈钢薄板焊接温度场与应力场的有限元数值分析模型．给出了运用 SYSWELD 软件的校正工具对双椭球体热源分布参数进行确定的方法．

（2）利用所建模型，对 GTAW 熔池形状从熔池开始形成到达到宏观准稳态这一动态演变过程进行了预测．计算结果表明，达到宏观准稳态时，计算结果与试验结果基本吻合．

参考文献：

[1] Orper G M, Eagar T W, Szekely J. Convection in arc weld pool [J]. Welding Journal, 1983, 62(11): 307s–312s.

[2] Ushio M, Wu C S. Mathematical modeling of 3-D heat and fluid flow in a moving GMA weld pool[J]. Metallurgical and Materials Transaction B, 1997, 28(2): 509–516.

[3] Hirata Y, Asai Y, Takenak K, et al. 3-D numerical model predicting penetration shape in GTA welding[J]. Materials Science Forum, 2003, 11(5): 426–432.

[4] Zhao P C, Wu C S, Zhang Y M. Numerical simulation of dynamic characteristic of weld pool geometry with step changes of welding parameters[J]. Modeling and Simulation in Materials Science and Engineering, 2004, 12(7): 765–780.

[5] Zacharia T, David S A, Vitek J M. Effect of evaporation and temperature-dependent material prosperities on weld pool development [J]. Metallurgical Transaction B, 1991, 22(4): 233–241.

[6] Goldak J, Chakravarti A, Bibby M. A double ellipsoid finite element model for welding heat sources[J]. Metallurgical Transactions B, 1984, 15B(6): 299–305.

[7] 李瑞英，赵 明，孙永兴．基于 SYSWELD 的不锈钢薄板 TIG 焊焊接三维温度场的有限元分析[J]．热加工工艺，2007, 36(19): 69–72.
Li Ruiying, Zhao Ming, Sun Yongxing. Finite element analysis of 3-D temperature fields on stainless steel sheet TIG welding based on SYSWELD software[J]. Hot Working Technology, 2007, 36(19): 69–72.

作者简介：李瑞英，女，1979 年出生，硕士研究生，讲师．主要研究方向为焊接热过程数值模拟．发表论文 3 篇．Email: lryd@126.com

通讯作者：赵 明，女，副教授．Email: meg10512001@yahoo.com.cn

welding methods (SMAW, TIG and SAW), and the microstructure mechanical property and corrosive property of welded joints are analyzed The results indicate that the phase ratio of ferrite in weld metal and heat-affected zone of the joints is controlled between 30%—60%, the tensile strength of the joints is near the same as that of base metal the impact absorbed energy of weld metal by TIG and SAW at −40 ℃ is 133 J and 78 J respectively higher than 37 J of SMAW significantly and impact absorbed energy of heat-affected zone in the joint welded by SAW at −40 ℃ is 207 J higher than 122 J of TIG and 109 J of SMAW because of its lowest total heat input In the temperature range from −60 ℃ to 20 ℃, the impact absorbed energy of weld metal and heat-affected zone in the joint welded by TIG is higher than that of SMAW. The pitting corrosion resistance of the joints welded by TIG and SAW is near the same better than that of SMAW. The comprehensive property of TIG joint is the best and then that of SAW, last the SMAW.

Key words: duplex stainless steel arc welding microstructure impact absorbed energy pitting corrosion resistance

Finite element analysis on 3-D molten pool geometry for GTAW based on SYSWELD software LI Ruiying, ZHAO Ming, ZHOU Hongyan (1 Department of Physics and Electricity Information Engineering Daqing Normal University Daqing 163712 China; 2 College of Mechanical & Electronic Engineering China University of Petroleum Dongying 257061, China). p 41—44

Abstract: A 3-dimensional transient numerical simulation model for gas tungsten arc (GTA) welding 0Cr18Ni9 stainless steel sheet was developed based on SYSWELD software A double ellipsoid heat source mode was adopted to depict the distribution of a moving GTA welding arc The method modified the parameters of heat source was put forward The thermo-physical properties and latent heat were taken into consideration The transient variations of temperature fields and molten pool geometry were predicted and verified It has been found that the calculated shape of molten pool was in agreement with the experimental one

Key words: double ellipsoid heat source molten pool geometry finite element method numerical simulation

Development of welding residual stress during postwelding heat treatment JIANG Wenchun, WANG Bingying, GONG Jianming (1 College of Mechanical and Electronic Engineering China University of Petroleum Dongying 257061 China; 2 School of Mechanical and Power Engineering Nanjing University of Technology Nanjing 210009 China). p 45—48

Abstract: The postwelding heat treatment (PWHT) is simulated by finite element method The results show that large as-weld residual stress is generated in the weld metal and heat affected zone (HAZ), and is decreased gradually far away the HAZ After PWHT the residual stress is decreased about 60%. PWHT not only decreases the residual stress but also makes the residual stress re-distributed The stress re-distribution makes the stress in base metal increase During the heating of PWHT the yield strength is decreased and the plastic deformation is generated which leads to the relaxation of residual stress During the cooling of PWHT the yield strength is increased which makes the stress increase The residual stress after PWHT is mainly generated during the cooling of PWHT The maximum residual stress is increased with the PWHT temperature increase but keeps stable above 600 ℃. Therefore a suitable temperature of 600 ℃ could be used in PWHT for Q345R steel

Key words: welding residual stress postwelding heat treatment finite element

Brazing of C_f/SiC and Ti alloy by using Ag-Cu-Ti active brazing alloy CAI Chuang, XIONG Jinhui, HUANG Jihua, CHEN Shuhai (School of Materials Science and Engineering University of Science and Technology Beijing Beijing 100083 China). p 49—51

Abstract: Carbon fiber reinforced SiC (C_f/SiC) was successfully joined to TC4 with Ag-Cu-Ti alloy powder by brazing The microstructures of the brazed joints were investigated with scanning electron microscope (SEM), energy dispersive spectrometer (EDS) and X-ray diffraction (XRD). The mechanical properties of the joints were measured with mechanical testing machine The results show that the joints mainly consist of TiC, Ti_3SiC_2, Ti_5Si_3, Ag, TiCu, Ti_3Cu_4 and Ti_2Cu reaction products TiC+ Ti_3SiC_2/Ti_5Si_3 + Ti_2Cu reaction layers are formed near C_f/SiC composite while Ti_3Cu_4/TiCu/Ti_2Cu/Ti_2Cu+ Ti reaction layers are formed near TC4 The maximum room temperature and 500 ℃ shear strengths of the joints are 102 MPa and 51 MPa at a brazing temperature of 900 ℃ and a holding time of 5 min

Key words: C_f/SiC, Ti alloy active brazing

Effect of laser shock processing on tensile strength of welded joints ZHOU Liucheng, ZHOU Lei, LI Yinghong, WANG Cheng (Air Force Engineering University Aero-Plasma Dynamic Laboratory Xi'an 710038 China). p 52—54 58

Abstract: The welded specimen of 12Cr2Ni4A stainless steel was shocked by pulse laser shock processing (LSP) as a post weld treatment technology once and twice and the Erichsen test surface residual stress and hardness of the welding joints of 12Cr2Ni4A stainless steel were compared before and after LSP treated The results indicate that the microhardness of the joints is improved by 50% after twice laser shock treated the tension strength is enhanced from 818.5 MPa to 863.8 MPa and the position of fracture transfers from heat-affected zone to parent material The LSP treatment can improve the tensile strength of the joints effectively and the eliminating of residual compressive stress makes great contributions to the improvement in fatigue properties of welding joints

Key words: laser shock processing surface treatment welding joints tensile strength

Analysis and evaluation of stainless steel flux-cored wire in vertical welding WANG Bin, LI Zhuoxin, LI Hong, LI Guodong (School of Material Science and Engineering Beijing University of Technology Beijing 100022 China). p 55—58

Abstract: Because the evaluation of wire vertical charac-